M. Danylenko, V. Kopylov, Yu. Podrezov, S. Firstov

STRUCTURAL SENSITIVITY OF THE MECHANICAL PROPERTIES OF Fe-Armco HIGH-DEFORMED BY THE EQUAL-CHANNEL ANGULAR PRESSURE

Institute for Problems of Materials Sciences
3 Krzhyzhanovsky St., 03142, Kyiv, Ukraine

The effect of ECAP deformation on the tensile stress-strain curves of high-deformed iron was studied. The influence of the deformation degrees on dislocation and cell structure evolution was analyzed. The structural sensitivity of the mechanical properties of high-deformed Fe-Armco was studied.

1. Introduction

The relationship between mechanical properties and laws governing dislocation substructure development during plastic deformation and other treatments of single-phase materials has received much attention from materials scientists over the past three decades. Detailed studies of the dislocation structure evolution [1] have helped to establish the characteristic stages in the evolution of defect structures and the corresponding changes in the deformation hardening mechanism. Strained BBC-metals have been shown to undergo internal structure evolution during plastic deformation over a wide range of temperature and deformation, Fig. 1.

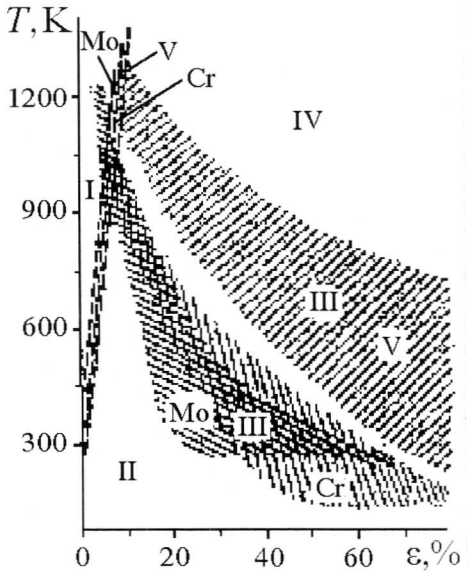

Fig. 1. Diagrams of structural states of BCC-metals: single dislocations and pile-up (I), chaotic distribution of dislocation (II), intermediate state (III), cell structure (IV) [1]

Change of microstructure due to plastic deformation at constant temperature occurs in the order: single dislocation pile up → low-angle cell structure → high-angle cell structure. These changes affect the process of strengthening during plastic deformation and mechanical properties of deformed materials. It was shown that

work-hardening curves for single structural states can be approximated by straight lines when the data are expressed by true stress σ versus square root of true strain $\sqrt{e}$ [2,3].

Bell [2] used this type of analysis to isolate the various stages of hardening (he called it quantization), but did not ascribe a structural basis to the observed effect. Moiseev et al. [3] revealed the staged nature of hardening (linear phases corresponding to different regions of the structural state diagrams). Fig. 2 shows a schematic representation of such diagram. Formally, each stage belongs to a deformation region with a new coefficient α in the expression

$$\Delta\sigma = \alpha G\mathbf{b}\sqrt{\rho}\,, \tag{1}$$

where G – shear modulus; $\mathbf{b}$ – Burgers vector; ρ – dislocation density; $\Delta\sigma$ – strengthening.

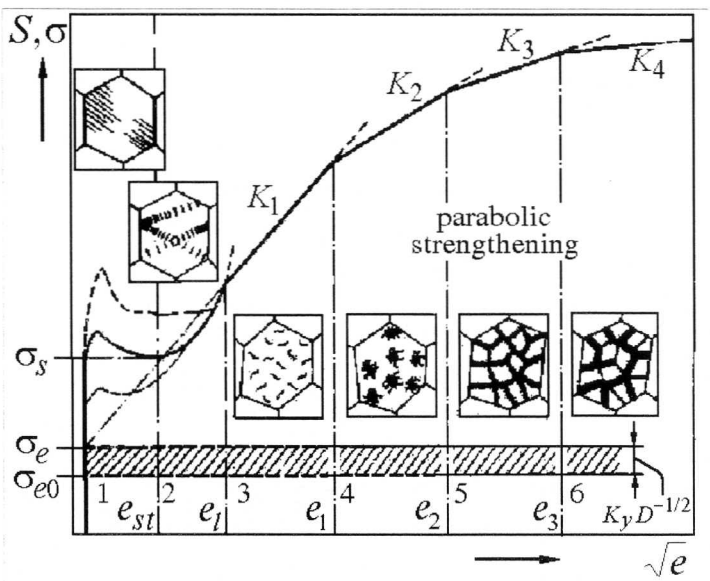

Fig. 2. Changes in the deformation hardening curve after recasting the data in terms of the coordinates $\sigma - \sqrt{e}$ [3]

A detailed discussion of the nature of hardening in each stage is beyond the scope of this paper. We simply note that parabolic strain hardening takes place, as a rule, at low and average degrees of deformation ($e < 1$).

2. Experimental Procedure

The science and technology of materials subject to severe plastic deformation (SPD) ($e > 1$) have evolved largely the past 10 years. Catalyzing contribution that gave birth to severe plastic deformation processing of materials was the work of Segal et al. [4], the inventor of equal-channel angular pressure (ECAP).

Segal proposed and demonstrated the concept of subjecting large volumes of material to simple shear in order to modify their microstructure and enhance properties.

2.1. Equal-channel angular pressure process

Equal-channel angular pressure is an innovative process capable of producing relatively uniform intensive plastic deformation in a variety of material systems, without causing substantial change in geometric shape of cross-section.

Fig. 3 illustrates the principle of ECA pressing. The die contains two channels, equal in cross-section, which intersect at an angle near the center of the die. The test sample is machined to fit the channels and pressed through the die with a plunger. The angle ϕ subtended by the two channels within the die is critical in determining the total strain accrued in the sample on each separate passage through the die. According to [4], plastic deformation degree is calculated from the expression

$$e = \text{arsh}(N \operatorname{ctg} \phi), \tag{2}$$

where N – pass number, ϕ – channel turn angle.

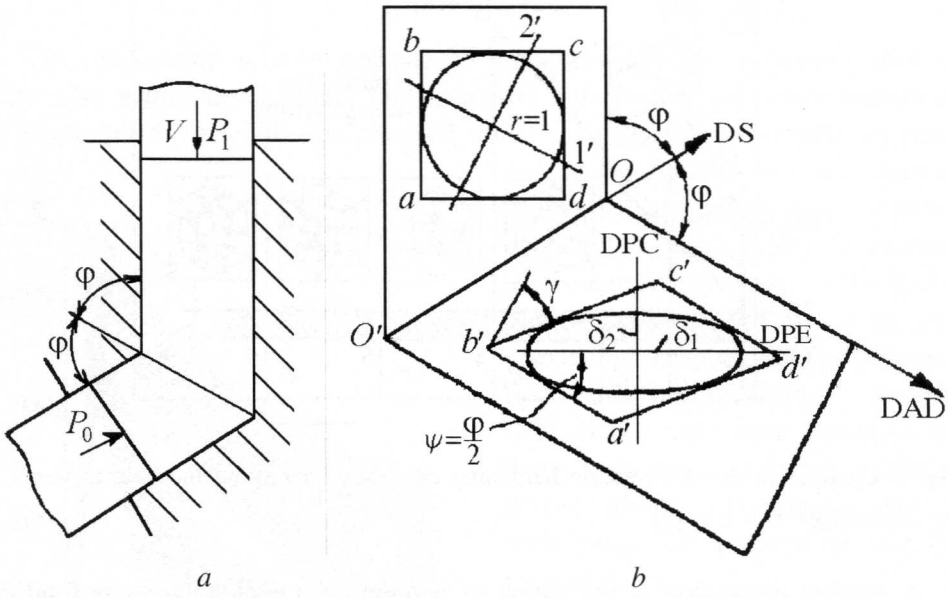

Fig. 3. ECAP scheme (*a*), ECAP process schematic showing billet shear (*b*): DAD – direct-axis direction, DS – direction of shear, DPE – direction of principal elongation, DPC – direction of principal compression

When samples are pressed repetitively it is possible to define some distinct processing routes. In route A the sample is not rotated between consecutive pressings, in route B it is rotated by 90° between each pressing were B_A denote rotation in alternate directions between each pressing and route B_C denotes rotation in the same direction between each pressing and route C denoted a rotation

of 180° between each pressing. The different processing routes give rise to different shearing characteristics within the sample and this leads to different microstructures.

The condition of ECAP deformation macrouniformity must be provided by special static boundary conditions on every deformation pass. These conditions depend upon the friction between the sample and press equipment, the contact area, and the special backpressure. Under these conditions the uniform deformation of simple shear arises on the line of channel interaction. If the special boundary conditions are not observed, non-uniform plastic flow occurs. Correct realization of ECAP deformation is named in [5] a clear ECAP. Clear ECAP technology was realized in Physical-Technical Institute of NAS of Belarus for severe plastic deformation of materials.

2.2. Test details

The strain hardening of iron at high plastic deformation (up to $e = 3$) has been investigated. The material selected for study was electrolytic vacuum-melted iron, containing 0.014% oxygen, 0.008% carbon and 0.0017% nitrogen. The starting sample dimensions for ECAP were 15×15×150 mm and the grain size 0.050 mm.

The effect of ECAP strain on the tensile stress-strain curves of high-deformed iron was studied. The route A was chosen as the main. The sequence of deformations corresponded to strain $e = 0.88$ per pass up to maximum strain of 2.89. In addition to the foregoing, two samples in route C (2 and 8 passes corresponded to strain of 1.35 and 2.65, respectively) and one sample in route B_C (8 passes corresponded to strain of 2.65) were deformed. A low and an average deformation degrees ($e = 0.05–1.0$) were obtained by rolling.

ECAP and tensile testing were carried out at room temperature. In the tensile test the strain rate was kept equal to 10^{-3} sec^{-1}. Fracture toughness was determined by three-point bending tests at 77 K [6]. The fracture energy was calculated using formula $\gamma_f = K_{1c}^2/2E$ (where γ_f – fracture energy; K_{1c} – fracture toughness; E – elastic modulus). Special extending grips [6] enabled to test specimens with crack introduced into the delamination plane.

Transmission electron micrographs were taken on both transverse and longitudinal sections. The cell (subgrain) sizes were determined by counting the number of cell-wall intercepts per unit length of traverse.

3. Experimental results

3.1. Tensile tests

The dependence of the strain hardening on plastic deformation degree for different deformation schemes is shown in Fig. 4. The true stress-strain curves are shown as a function of total strain, which includes both the ECAP and the tensile deformation testing. None of the ECAP samples exhibited more than 1%

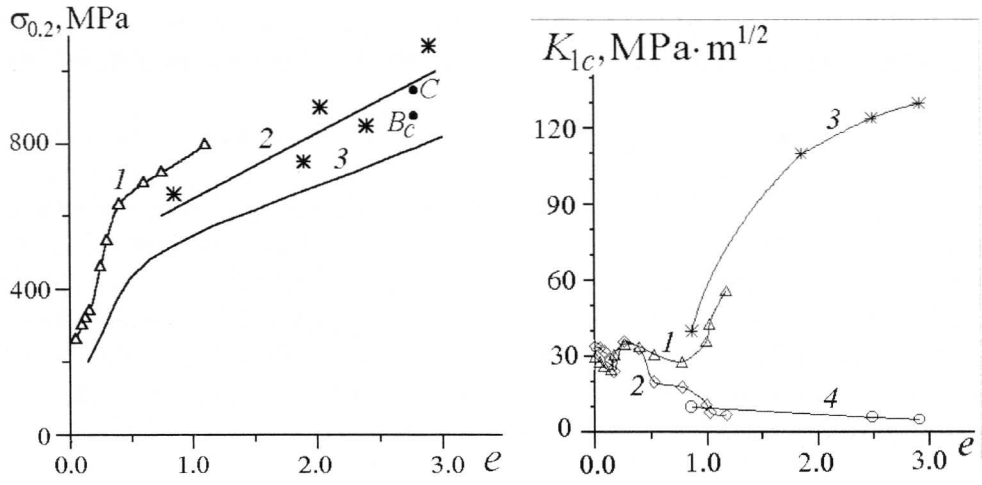

Fig. 4. Effect of strain on yield point of rolled (1), ECAP (2) materials and drawn wires [7] (3)

Fig. 5. Fracture toughness of strained iron: *1*, *2* – rolling; *3*, *4* – ECAP (*1*, *3* – crack introduced into the plane perpendicular to the plane of deformation; *2*, *4* – crack introduced into the plane parallel to the plane of deformation)

uniform elongation before necking. The envelope of stress-strain curves in Fig. 4 represents the work-hardening behavior during continuous deformation.

The parabolic strain hardening was found at a low and at an average deformation degrees and the linear stage of deformation took place at high deformation degrees. The experimental yield point for different ECA-press schemes gives general dependence (Fig. 4, curve *2*). That is followed by a few influence of an ECA-press schemes on the strain hardening. The strain hardening after the rolling (Fig. 4, curve *1*) shows some more intensity. That is because of more capacity for shift deformation, which gives recovery effect. But this recovery effect is less than in Langford experiment (Fig. 4, curve *3*) where strain hardening for the drawn wires was investigated.

3.2. Fracture toughness

In our previous works [6,8] the effect of dislocation structure on fracture toughness and mechanisms of fracture of BCC-metals have been studied.

One can distinguish certain sections limited by bounds of the structural states of the deformed materials on the graphs: in the interval of low deformation degrees (interval I), which is characterized by chaotic distribution of dislocations, the fracture toughness decreases with the deformation growth; the origin of the cells with low-angle boundaries (interval II) results in the sharp increase of the fracture toughness; when cells with the low-angle boundaries exist the fracture toughness demonstrates the next decrease (interval III), and, at last, when misoriented cells develop the growth of the fracture characteristic for specimens with

cracks introduced into the plane perpendicular to the plane of deformation and, contrary, decreasing of the fracture characteristic for specimens with cracks introduced into the plane parallel to the plane of deformation were observed (interval IV).

In [6] we investigated the influence of a deformation degree on fracture toughness in electrolytic vacuum-melted iron. Fracture toughness was determined by bending the specimens with cracks introduced into the plane perpendicular to the plane of deformation and into the plane parallel to the plane of deformation. This is shown in Fig. 5 (curve *1* for specimens with cracks introduced into the plane perpendicular to the plane of deformation, curve *2* for specimens with cracks introduced into the plane parallel to the plane of deformation).

ECAP process gives a possibility to investigate fracture toughness of high-deformed materials (interval IV) more carefully. Experimental data are shown in Fig. 5 (curve *3* for specimens with cracks introduced into the plane perpendicular to main deformation direction, curve 4 for specimens with cracks introduced into the plane parallel to the plane of the main elongation). This data demonstrate essential sensitivity of the fracture energy to structural evolution under high deformation degrees.

3.3. Substructural observation

Transmission electron microscopy takes transverse and longitudinal section of deformed samples. The mean transverse linear-intercept cell sizes measured on electron micrographs are plotted vs strain in Fig. 6. It is evident that the cells continue to undergo refinement in cross section up to the maximum plastic strain reached.

The cells begin to form during deformation process at a strain of about 0.2 μm and tend to take the elongated ribbon shape with further reduction of dimensions. There are important departures from this behavior. First, because of polygonization (formation of cell walls) which increases the number of cells. Second, because of dynamic recovery (via cell wall migration) which decreases the number of cells. Both of these phenomena prevent the width–thickness ratio of the cellular cross section. As is known [9], the cells in deformed iron start with equiaxed shapes and then become ribbon-like in cross section under deformation.

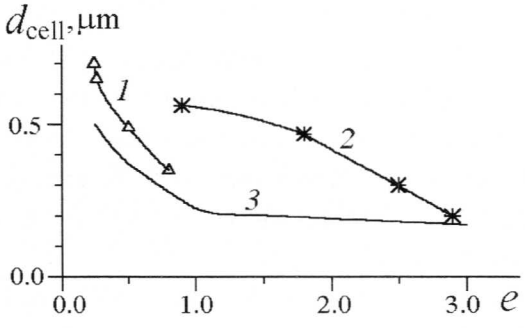

Fig. 6. Effect of strain on cell size of rolled (*1*), ECAP (*2*) materials and drawn wires [7] (*3*)

One can write the following expression for *f*-parameter, the

fraction of the initial number of cells in a cross section at any given amount of strain:

$$f = \frac{n}{n_i} \exp[-(e - e_i)], \tag{3}$$

where n_i is the initial number of cells per unit cross-sectional area as formed at some early strain e_i and n is the number of cells per unit cross-sectional area at some subsequent stain e. Measurements of n have been made during the deformation and corresponding values of f-parameter vs e are plotted in Fig. 7. As it can be deduced from Fig. 7, f is near unity for both wire drawing [7] and rolling deformation under low and average deformation degrees. This result is in a good agreement with Taylor–Pollany law: both bulk material and structural elements (grains, cell) have the same shape changing under deformation. Since ECAP is a process capable of producing plastic deformation without causing substantial change in geometric shape of billet, the cell size of ECAP deformed iron at the average deformation degrees is substantially larger.

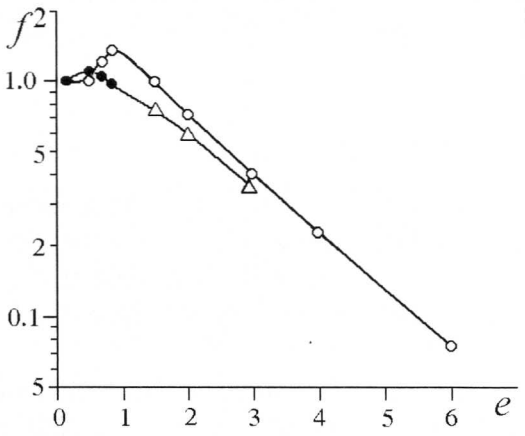

Fig. 7. The dependence of f-parameter on deformation (• – rolling, Δ – ECAP, o – [7])

Under high deformation degrees, principal changing in f vs e dependence take place. There is the large decrease in f throughout the subsequent elongation, signifying that substantial dynamic recovery is operative during the cell refinement. This means that many cells are being lost from the structure simultaneously with cross-sectional reduction of the remaining cells. It is clear that cell wall migration constitute very important aspect of the structural changes and critical deformation degree e_c under which changing in f vs e dependence take place is very important quantity.

Cell size evolution under deformation is accompanied with increasing of cell misorientation. In [10] there is a series of histograms showing the distribution of cell misorientations as a function of deformation. It was noted that distribution of misorientations Φ widens under plastic deformation and its average value rises with increasing strain (Fig. 8). Our experimental results are in a good agreement with Φ vs e dependence in [10].

The appearance of misoriented boundaries of cells in deformed BCC-metals changes their behavior. The stress τ, which is necessary for overcoming the boundary of cells by dislocation slipping depends on the angle of misorientation Φ_p

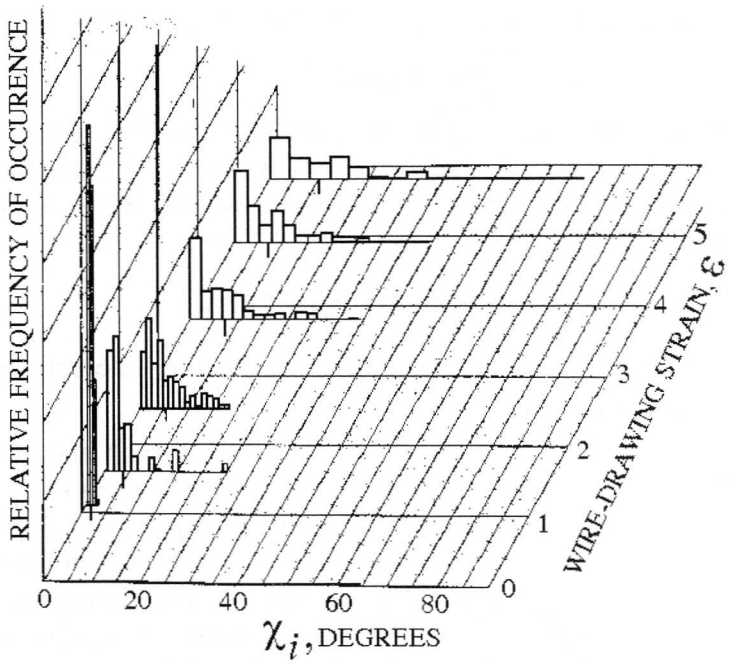

Fig. 8. Cell misorientation as a function of wire-drawing strain [10]

$$\tau = \Phi_p G/2\pi, \tag{4}$$

where G – shear modulus. According to [11] for Φ_p = 3°, the boundary of cells is a strong barrier for slipping. That is exactly the average misorientation value, which has cellular substructure under critical deformation e_c.

Thus, the substructure development under plastic deformation is characterized by the coexistence of two different size and misorientation scales, namely of a cell structure and a subgrain structure.

4. Discussion

Conventional grain size models are based on dislocation initiation or source activation as the critical stage in determining the strength and this model leads to the Hall–Petch equation

$$\sigma_y = \sigma_{y0} + kd^{-1/2}. \tag{5}$$

For the case of cells produced at low temperature the analysis of Holt [12] should apply. He showed that the wavelength of dislocation density, which becomes the cell size, varies with ρ as

$$d = \frac{K}{\sqrt{\rho}}, \tag{6}$$

where K is a constant for a given material. The combination of Eqs. (1) and (6)

leads to

$$\Delta\sigma = \alpha KGbd^{-1}. \tag{7}$$

Experimental data (Fig. 4 and Fig. 6) give the possibility to analyze the dependence of yield point of high-deformed Fe-Armco on the average cell size. This dependence is shown in Fig. 9. The dependence has a good approximation by equation

$$\sigma_y = \sigma_{y0} + md^{-1} = 200 + 0.230d^{-1}, \tag{8}$$

where σ_y – yield point; d – average cell size; m – strain hardening coefficient; σ_{y0} – undeformed hardening.

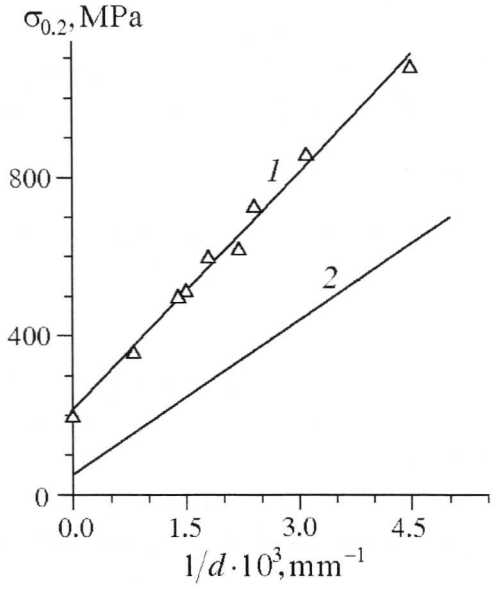

Fig. 9. Effect of cell size on yield point of rolled and ECAP (*1*), Langford [7] (*2*) materials

One of such models was proposed by Langford [7]. Cell size strengthening given by Eq. 2 can be accounted for on the assumption that the dislocation sources in the cell walls are readily activated at low applied stress (with the aid of high stress concentration) and that the observed strain hardening arises from the stress required to expand each of dislocation loops across the glide plane on the cell until the loop is incorporate in, or annihilated at the perimeter of the glide plane. The increase in cell length per passage of a dislocation is $\Delta l = (2/3)^{1/2}\mathbf{b}$ where $\mathbf{b}$ is Burgers vector. The numerical factor stems from the angle between the (111) slip direction and the wire axis in the ⟨110⟩ texture. The strain per passage of a dislocation is then

$$\Delta\varepsilon_d = \sqrt{2/3}(b/l), \tag{9}$$

where l is the length of the cell and the corresponding work of deformation per unit cell volume is $\Delta\varepsilon_d\sigma$, σ being tensile slow stress.

We now set $\sigma\Delta\varepsilon_d$ equal to the energy per unit volume expended in forcing the expanding dislocation loop against the friction stress (σ_0) on the glide plane plus the energy per unit volume required to generate the total length of dislocation line (which grows from nil to the perimeter of the glide plane). If slip takes place on {110} in the textured structure, the perimeter of the elliptical glide

plane is $1.54P$, where P is the approximately equiaxed cross-sectional perimeter of the cell. Then,

$$\sigma\Delta\varepsilon_d = \sigma_0\Delta\varepsilon_d + \frac{1.54P\Gamma}{AL}, \tag{10}$$

where A is the cross-sectional area of the cell, AL is the cell volume, and Γ is the energy per unit length of dislocation line. Substituting for $\Delta\varepsilon_d$:

$$\sigma = \sigma_0 + 1.54\sqrt{3/2}(P/A)(\Gamma/b), \tag{11}$$

From quantitative metallography,

$$P/A = \pi/\bar{d} \tag{12}$$

and so

$$\sigma = \sigma_0 + 1.54\pi\sqrt{3/2}\left(\Gamma/\bar{d}b\right). \tag{13}$$

A conservative estimate for $\Gamma = G\mathbf{b}^2/2$, and then

$$\sigma = \sigma_0 0.77\pi\sqrt{3/2}\left(Gb/\bar{d}\right), \tag{14}$$

$$\sigma = \sigma_0 3.0\, Gb/d\,. \tag{15}$$

Thus, the proposed model predicts a linear dependence of the strength on $\left(\bar{d}\right)^{-1}$ in conformity with Fig. 4. The theoretical slope is $3.0Gb$ compared to $5.9Gb$ observed experimentally by Langford [7] and $9.4Gb$ observed experimentally under ECA-press. The friction stress given by the empirical Eq. 2 is in the range expected for iron, but is very small compared to the $\left(\bar{d}\right)^{-1}$ term. In the model [7] most of the work of deformation goes into the generation of the total dislocation length necessary to produce the imposed plastic elongation of the cells. These dislocations have three fates: (a) loss by annihilation at (or) in the cell walls, (b) loss by the growth of cells, and (c) incorporation in the remaining cell walls (stored energy). The quantity ($3.0Gb/\bar{d}$) in Eq. 15 is the reversible work to generate these dislocations and is therefore a lower bound to the solution. Thus, the slope of the (σ vs $1/\bar{d}$) curve given by Eq. 15 can be expected to be somewhat lower than the experimental slope.

It is evident that the strength of subgrains can be independent of misorientation; in this case the Holt's equation is valid. This statement is in good agreement with our experimental data (Fig. 8). According to the Langford's model cells demonstrate «low-angle» hardening within the entire range of deformation. Cell-wall loosing which takes place under high deformation ($e > e_c$) is affected by dynamic recovery. In this case a linear stage of strengthening appears as the result of the loss of hardening under recovery. Thus, transition from parabolic stage of strain hardening to a linear one is not related with the change of a de-

formation mechanism.

In contrast, the increase of the deformation degree ($e > e_c$) promotes the change of the failure mechanism: quasi-cleavage → quasi-cleavage with delamination. The growth of the fracture toughness for specimens with cracks introduced into the plane perpendicular to the plane of deformation and vice versa – the decrease of the fracture characteristic for specimens with cracks introduced into the plane parallel to the plane of deformation are related with the change of the fracture mechanism (Fig. 5).

Fractography analysis by REM method shows that in the case of highly deformed Fe-Armco under delamination failure conditions crack propagates along boundaries of the cells whose longitudinal axes coincide with the main deformation direction (Fig. 6). At high deformation degrees the crack does not move in the straight direction; it turns in the delamination plane and propagates along the cell wall. Since the plane of main elongation has different orientation with respect to the sample axis for different deformation degrees, the angle of crack turning increases with deformation according to the scheme shown in Fig. 3.

Interaction of the crack with a weakened grain boundary whose plane does not coincide with the crack plane has been studied in [13,14]. The dependence of grain boundary energy on the value of the crack deflection angle was studied for unalloyed tungsten. The results of the experiment are shown in Fig. 10,*a*. Fracture toughness of grain boundary increases with increasing of the deflection angle value. In polar coordinates the dependence $1/K_{1c}$ vs Φ (where Φ – the deflection angle value) agrees with the theoretical angular dependence of stress distribution at the tip of the crack [15].

It was established that fracture toughness in this case can be obtained from the equation

$$K_{1c}(\Phi) = K_{1c}^{b} f(\Phi), \tag{15}$$

where K_{1c} – the fracture toughness of the material whose grain boundaries are rotated through an angle Φ with the plane of the crack; K_{1c}^{b} – the fracture toughness in the plane of a grain boundary; $f(\Phi)$ – the angle function, which takes into account stress distribution at the crack tip.

Experimental data (Fig. 4) can be transformed in accordance with Eq. 10 taking into account that K_{1c} is the fracture toughness of material with cracks introduced into the plane perpendicular to the plane of deformation and K_{1c}^{b} is the fracture toughness in the delamination plane (this value is close to the fracture toughness of cell walls). These results are given in Table.

$1/K_{1c}$ vs Φ diagram for highly deformed iron is shown in Fig. 10,*b*. At the first sight these data are in good agreement with the model of crack interaction with weakened grain boundary (Fig. 10,*a*). But in the investigated case we take into account two substantial features of fracture mechanisms.

Table

e	Φ, deg	Route	K_{1c}, MPa·m$^{1/2}$	K_{1c}^{b}, MPa·m$^{1/2}$	$f(\Phi)$	Fracture mechanism
0.88	30	A	40	14	3	cl. + del.
1.64	60	A	97	9	10	del.
2.6	70	A	120	7	17	del.
2.96	80	A	130	6	22	del.
2.80	30	C	28	7	4	del.
2.80	40	B_c	40	8	5	del.

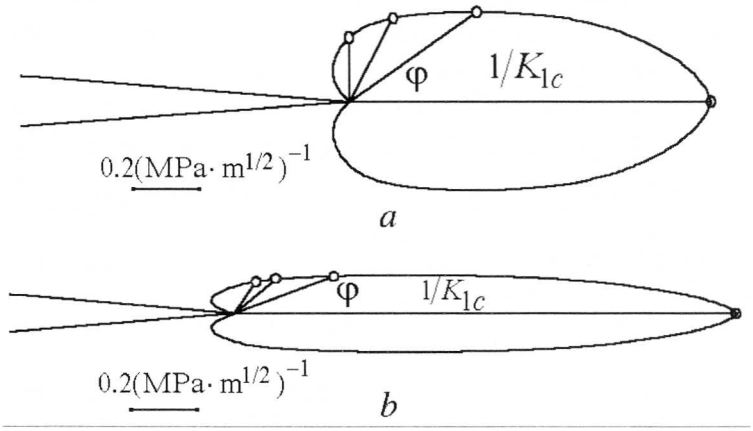

Fig. 10. $1/K_{1c}$ vs Φ diagram: a – intercrystalline fracture, b – intercell fracture

The first is that in our experiments the ratio K_{1c}/K_{1c}^{b} for given Φ essentially exceeds the value of this parameter obtained from the grain boundary test [13] or from the Irvin's theory estimation [15].

The second is that crack turning in the delamination plane under $e > e_c$ requires considerably more fracture energy compared with trans-crystalline (grain or cell) fracture under lower ($e < e_c$) deformation. It seems that the crack cannot propagate across the nano-crystalline misoriented cells. More careful investigations are required to clear the problem.

5. Conclusions

1. Critical deformation e_c is associated with the beginning of severe plastic behaviour of deformed materials.

2. Substructure development under high plastic deformation is characterized by the coexistence of two different size and misorientation scales:

– at e_c the change in f vs. e dependence takes place. Many cells are lost si-

multaneously with cross-sectional reduction of the remaining cells;

– cell size evolution under high deformation is accompanied with increasing of the cell misorientation. Critical misorientation Φ_p at which the boundaries of cells are strong barriers for slipping is exactly the average misorientation value at critical deformation e_c.

3. The change of mechanical behavior of deformed materials near critical deformation e_c takes place:

– the parabolic strain hardening which was observed at the low and average deformation degrees was changed by the linear stage of deformation at high deformation degrees;

– the growth of the fracture toughness for specimens with cracks introduced into the plane perpendicular to the plane of deformation was shown;

– decreasing of the fracture characteristic for specimens with cracks introduced into the plane parallel to the plane of deformation was observed.

4. Transition from the parabolic stage of strain hardening to the linear one is not related with the change of the deformation mechanism. In contrast, increasing of the deformation degree ($e > e_c$) promotes the change of the failure mechanism: quasi-cleavage → quasi-cleavage with delamination.

1. *V.I. Trefilov, Yu.V. Milman, S.A. Firstov*, Physical Principles of Strength of Refractory Metals, Naukova Dumka, Kiev (1975) [in Russian].
2. *J. Bell*, Experimental Bases of the Mechanics of Deformed Bodies, Part 1, London (1984).
3. *V.I. Trefilov, V.F. Moiseyev, A.P. Pechcovsky*, Work Hardening and Fracture of the Polycrystal Metals, V.I. Trefilov (ed.), Naukova Dumka, Kiev (1975) [in Russian].
4. *V.M. Segal, V.I. Reznikov, V.I. Kopilov, D.A. Pavlik, V.F. Malyshev*, Processes of Plastic Structural Formation of Metals, Nauka i technika publishers, Minsk (1994) [in Russian].
5. *V.I. Kopilov*, in: Proc. of NATO ARW, Moscow, Russia, T.C. Lowe, R.Z. Valiev (eds.), Kluwer Academic Publishers, Netherlands (1999), pp. 23–29.
6. *M. Danilenko, A. Demidik, Yu. Podrezov, A. Rashek*, Sov. Powder Metallurgy and Metal Ceramics **30**, 780 (1991).
7. G. Langford, M. Cohen, Trans. ASM **62**, 623 (1966).
8. *M. Danilenko, Yu. Podrezov, S. Firstov*, Theor. Appl. Frac. Mech. **32**, 9 (1999).
9. *R.C. Clenn, G. Langford, A.S. Keh*, ASM Trans. Quan. **62**, 285 (1969).
10. *G. Langford, M. Cohen*, Met. Trans. **6A**, 901 (1975).
11. *D. Read*, Dislocations in Crystals, McGraw-Hill, New York, London, Toronto (1955).
12. *D.T. Holt*, J. Appl. Phys. **41**, 3197 (1970).
13. *A.S. Drachinski, Yu.N. Podrezov, V.I. Trefilov*, FMM **52**, 417 (1981) [in Russian].
14. *M. Danylenko*, in: Proc. of the127th Annual Meeting of the Minerals & Materials Society, E.M. Talleff, R.K. Mahidhara (eds.), San Antonio, Texas, 12–19 February, 1998, pp. 229–235.
15. *G.R. Irwin*, Fracturing of Metals ASM, Cleveland (1948).